Journal Name: Hydrology and Earth System Sciences

Supplementary Material for "Characterizing runoff response to rainfall in permafrost catchments and its implications for hydrological and biogeochemical fluxes in a warming climate"

Cansu Culha[1], Sarah Godsey[2], Shawn Chartrand[3], Melissa Lafrenière[4], James McNamara[5], James Kirchner[6,7]

[1] Department of Earth, Ocean and Atmospheric Sciences, University of British Columbia, Vancouver, BC V6T 1Z4, Canada
[2] Department of Geosciences, Idaho State University, Pocatello, ID 83209, USA
[3] Department of Geography, Simon Fraser University, Burnaby, BC V5A 1S6, Canada
[4] Department of Geography and Planning, Queen's University, Kingston, ON K7L 3N6, Canada
[5] Department of Geosciences, Boise State University, Boise, ID 83725, USA
[6] Department of Environmental Systems Science, ETH Zürich, Zürich, 8092, Switzerland
[7] Swiss Federal Research Institute WSL, Birmensdorf, 8903, Switzerland

Correspondence to: Cansu Culha (cansu.culha@gmail.com)

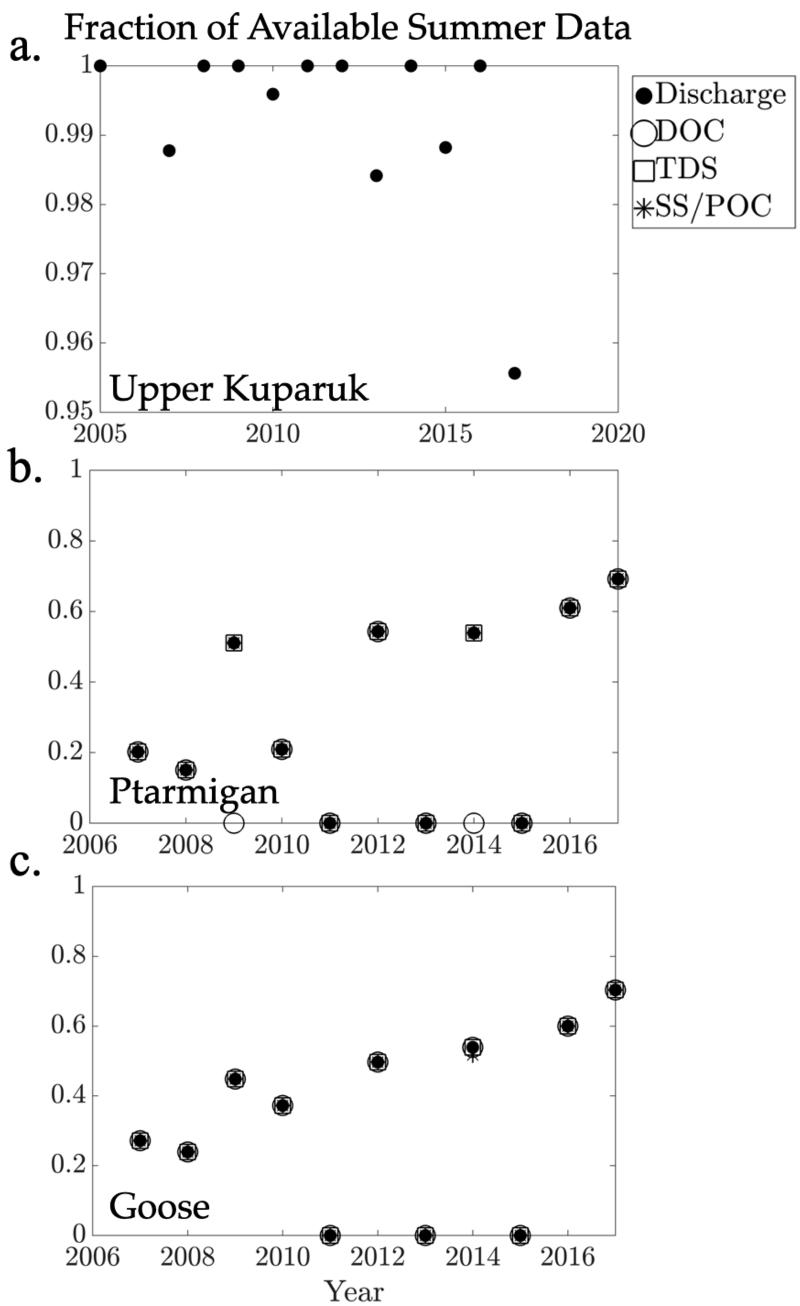

Supplementary Figures

Supplementary Figure 1. Fraction of available data during the summer months for the Upper Kuparuk (a), Goose (b), and Ptarmigan (c) catchments. Solid markers indicate discharge data availability, while open circle markers represent material fluxes data availability. Among the three sites, Upper Kuparuk (a) has the most consistent coverage, with over 95% discharge data availability in most years. In contrast, both Goose (b) and Ptarmigan (c) catchments at Cape Bounty include material flux data but have less consistent overall coverage.

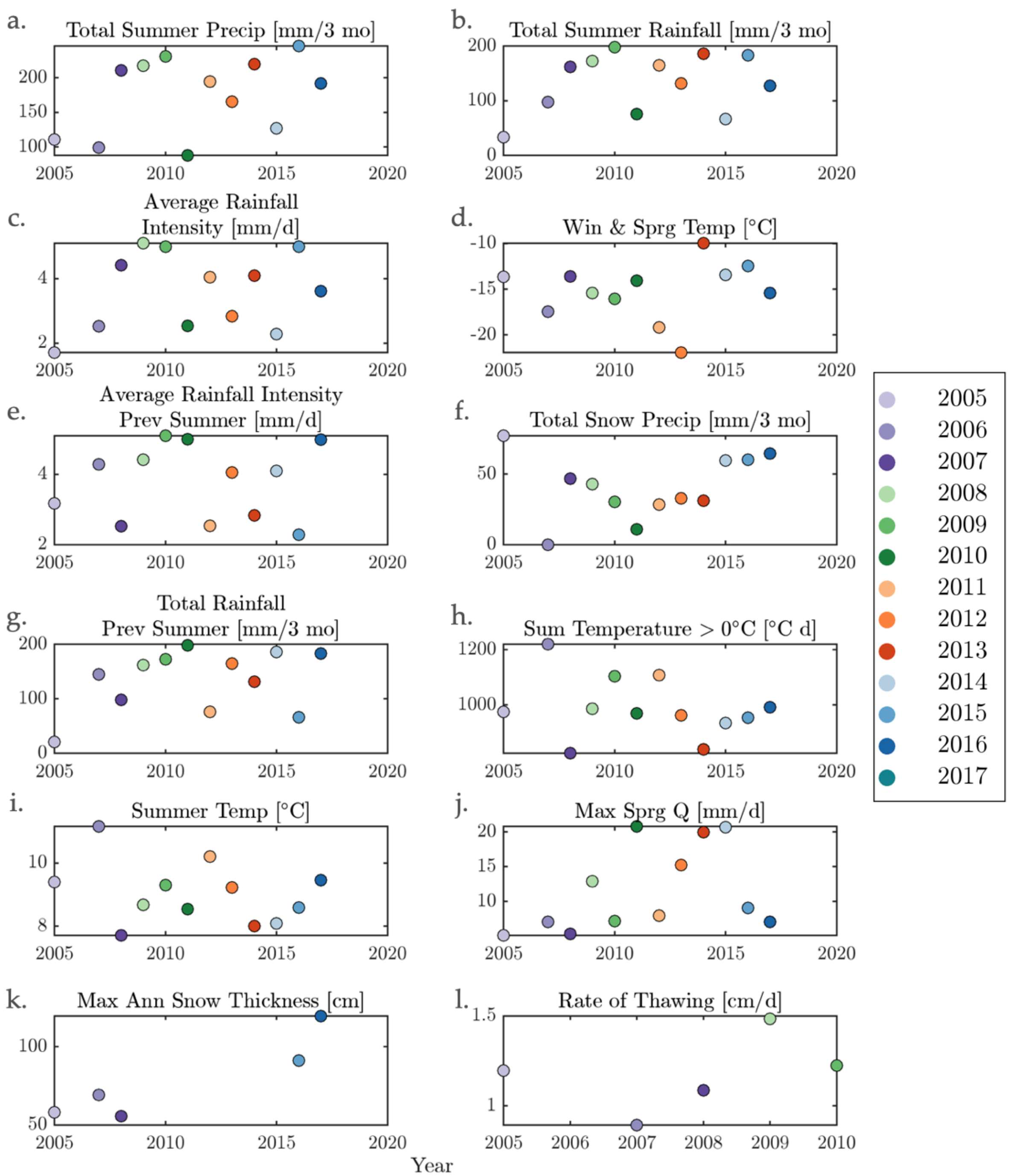

Supplementary Figure 2. Time series of potential explanatory variables for runoff response at Upper Kuparuk. Each color represents a distinct year and is used consistently throughout the manuscript. To improve visual grouping, we use light to dark shading within a color family to represent three consecutive years before switching to a new base color. We evaluate 12 potential explanatory variables: (a) total summer precipitation, (b) total summer rainfall, (c) average rainfall intensity, (d) average temperatures during the preceding winter and spring, (e) average rainfall intensity of the previous summer, (f) total snowfall, (g) total summer precipitation of the previous summer, (h) cumulative number of degree days above 0°C, (i) average summer temperature, (j) maximum spring streamflow, (k) maximum snow depth, and (l) rate of thawing. The plot titles correspond to the y-axis. Full descriptions of how each variable was derived are provided in the Methods section. Note that maximum snow depth and rate of thawing are only available for five years and are included as context.

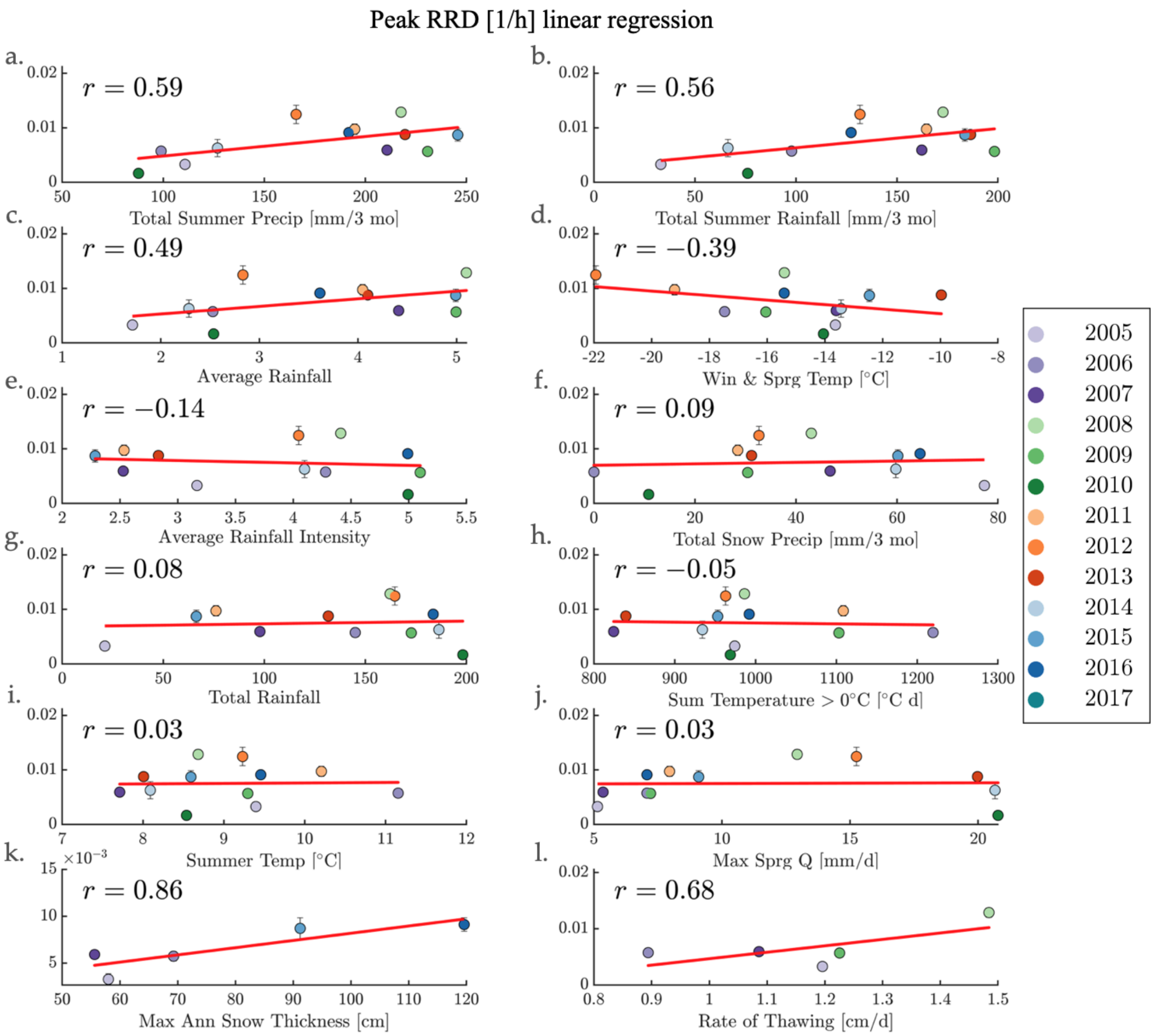

Supplementary Figure 3. Linear regression between each explanatory variable in Supp. Fig. 2 and runoff response distribution (RRD) peak height at Upper Kuparuk. The potential explanatory variables are shown along the x-axis: (a) total summer precipitation, (b) total summer rainfall, (c) average rainfall intensity, (d) average temperatures during the preceding winter and spring, (e) average rainfall intensity of the previous summer, (f) total snowfall, (g) total summer precipitation of the previous summer, (h) cumulative number of degree days above 0°C, (i) average summer temperature, (j) maximum spring streamflow, (k) maximum snow depth, and (l) rate of thawing. Note that maximum snow depth and rate of thawing are only available for five years and are included as context.

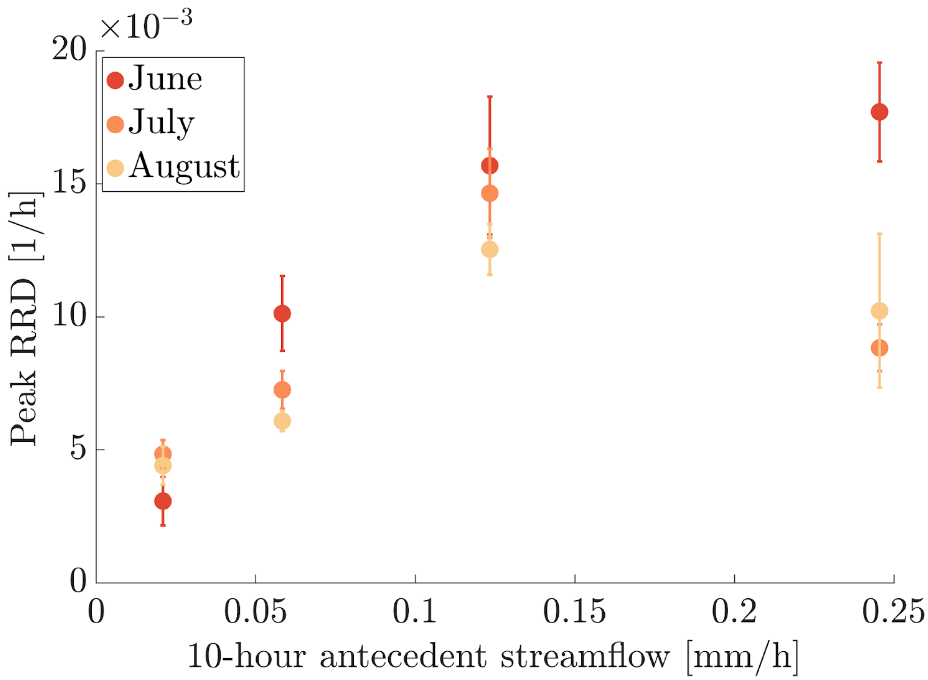

Supplementary Figure 4. Peak runoff response as a function of antecedent streamflow, showing that runoff is more sensitive to antecedent streamflow than to the month in which it occurs. We bin peak runoff responses by antecedent streamflow and compare the results across June, July, and August. The antecedent streamflow binning is the same as in **Man. Fig. 2**. In all months, peak runoff response increases with antecedent streamflow, except in the highest bin, which is based on fewer events: 44 for June, 38 for July, and only 11 for August. By contrast, the other bins each contain an average of 50 events. Across all bins, the months exhibit similar peak runoff responses, with the lowest responses occurring at the lowest antecedent streamflow. June displays the highest peak runoff response at high antecedent streamflow levels.

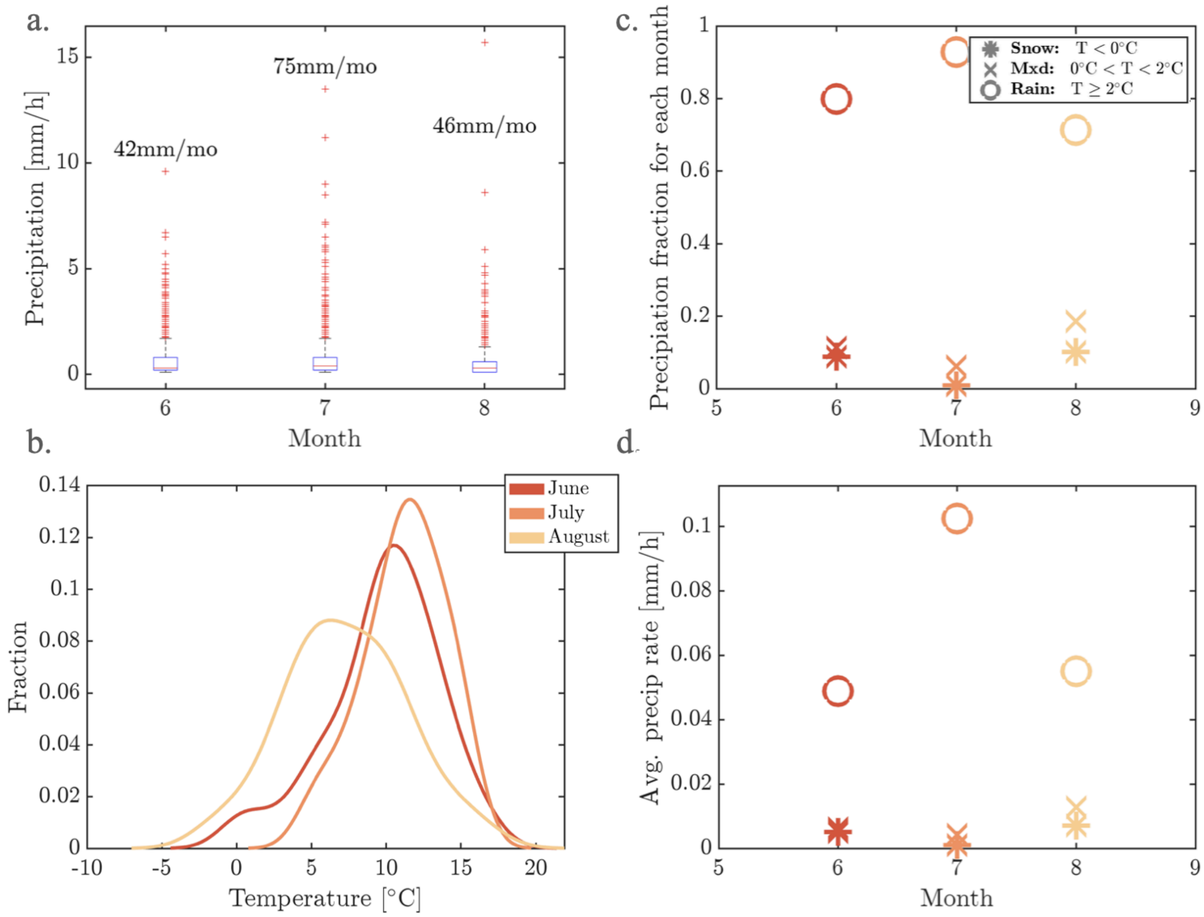

Supplementary Figure 5. Rainfall and temperature patterns across summer months (June is red, July is orange, and August is yellow). (a) The average precipitation for each hour with nonzero precipitation; cumulative monthly precipitation is shown above each boxplot. (b) Hourly temperature distribution for each month. (c) Average hourly precipitation by precipitation type, classified by temperature during precipitation. (d) Average precipitation rate per hour with rain. Note that higher precipitation rates in July (panel d) do not necessarily yield proportionally higher monthly totals (panel a), as total precipitation also depends on the duration of rainfall events. Circle, cross and star correspond to rain, mixed precipitation, and snow, respectively, in (b) and (d).

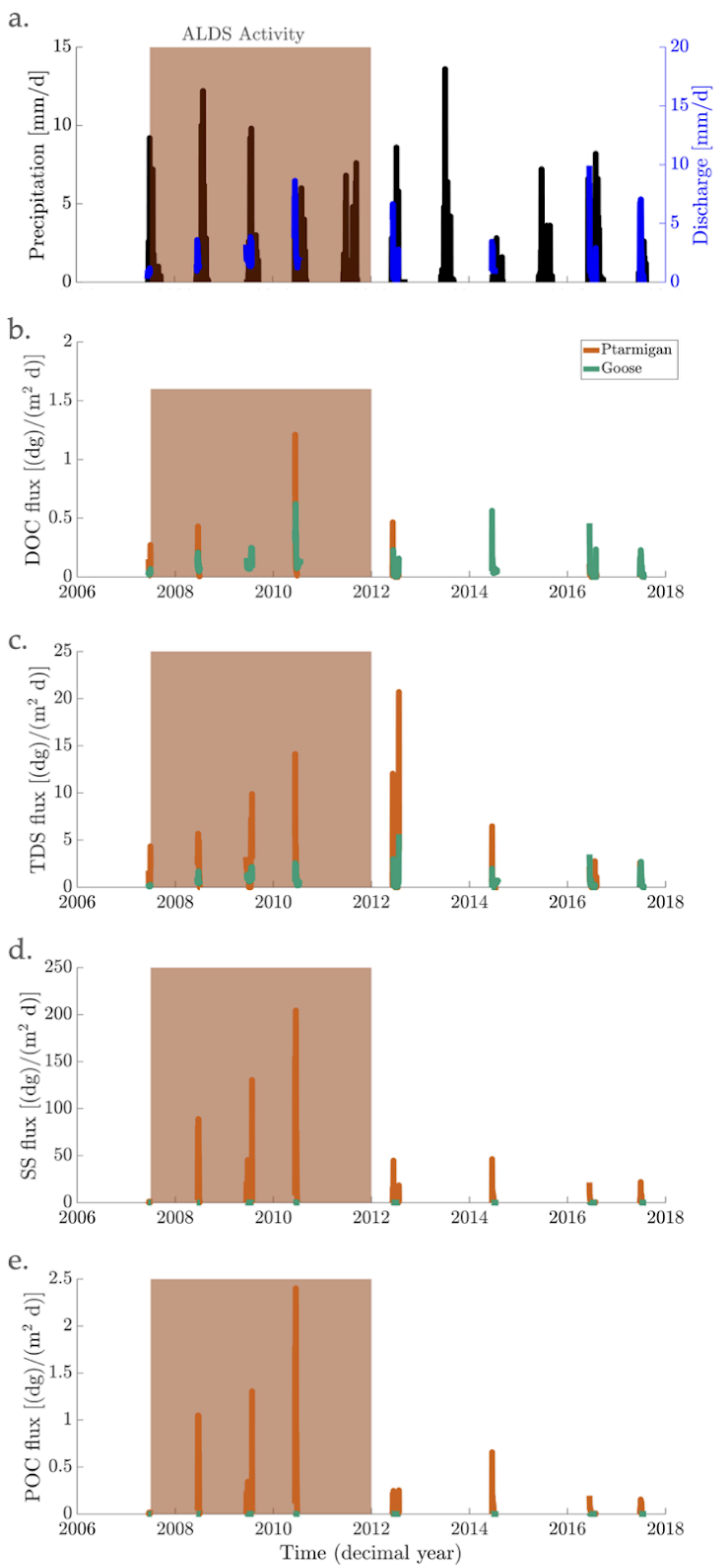

Supplementary Figure 6.Time-series comparison of daily precipitation, discharge, and material fluxes at the Ptarmigan catchment (with active layer detachments (ALDs), orange) and the Goose catchment without ALDs, green). The light-brown shading (late-2007 to 2011) delineates the interval when active layer detachments (ALDs) are actively eroding at Ptarmigan. Panel (a) shows daily totals of summer precipitation (black) and discharge (blue). Panels (b)–(e) present dissolved organic carbon (DOC), total dissolved solids (TDS), suspended sediment (SS), and particulate organic carbon (POC) fluxes, respectively; fluxes are calculated as concentration multiplied by discharge and are expressed as milligrams of material per area per day (mg m^{-2} d^{-1}). During the ALD interval, DOC flux is elevated at Ptarmigan but subsequently declines such that Goose becomes the larger DOC source. TDS flux is persistently higher at Ptarmigan and rises further while the slides are active. SSC and POC fluxes at Ptarmigan increase by an order of magnitude during ALD activity, whereas both fluxes remain minimal at Goose throughout the record.

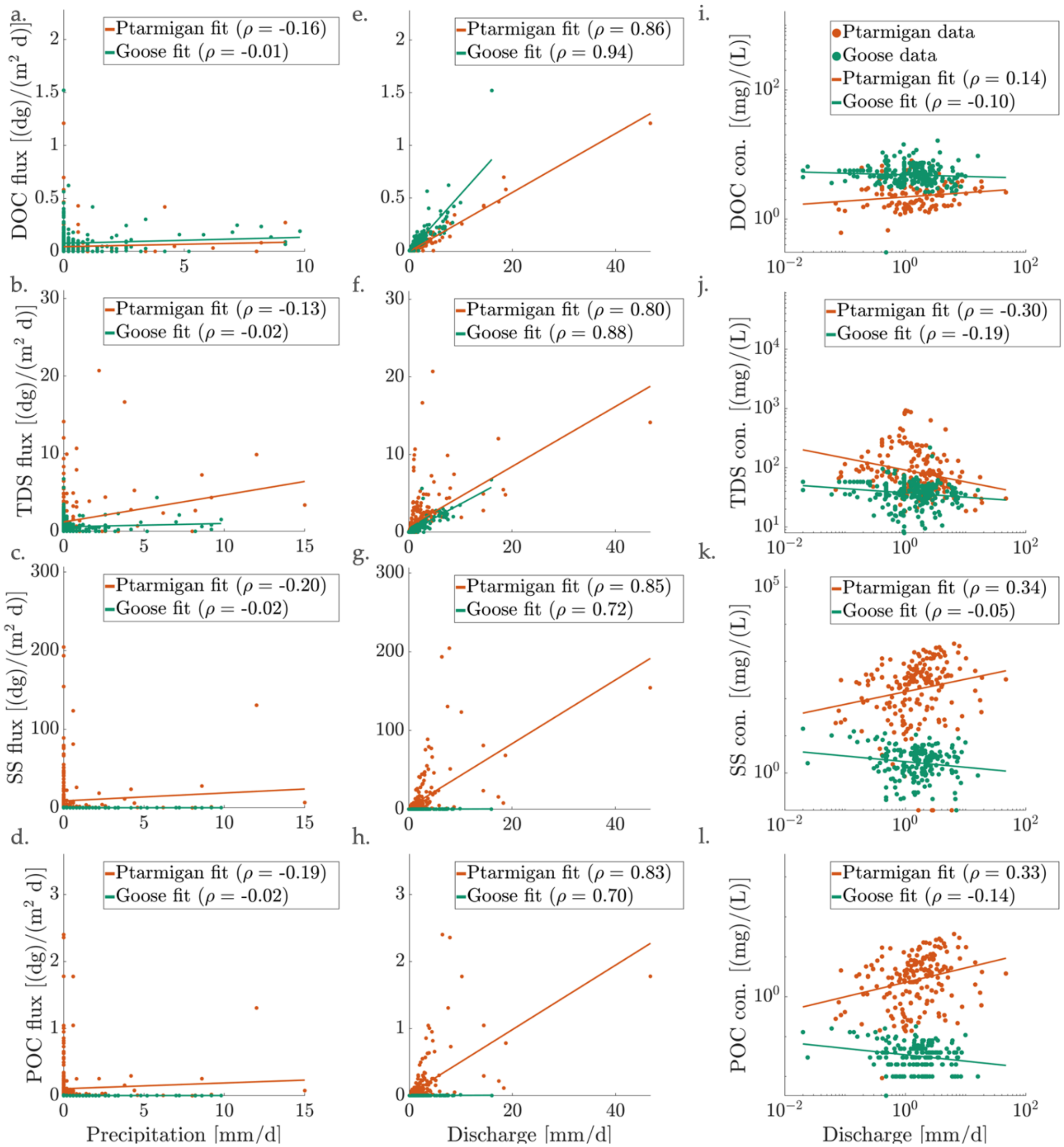

Supplementary Figure 7. Correlation between precipitation [(a)–(d)] and discharge [(e)–(h)] with material fluxes [(a)-(h)] and concentrations [(i)-(l)] in the Ptarmigan catchment (with active layer detachments [ALDs], orange) and the Goose catchment (without ALDs, green). Panels show dissolved organic carbon (DOC), total dissolved solids (TDS), suspended sediment (SS), and particulate organic carbon (POC) fluxes and concentrations. Panels [(i) - (l)] are log-log scale. There is no clear correlation between precipitation and material fluxes, as well as, discharge and material concentrations at either catchment. In contrast, discharge shows a positive correlation with material flux, particularly for TDS, SS, and POC at Ptarmigan. Goose shows higher DOC flux with increasing discharge, while Ptarmigan exhibits greater TDS, SS, and POC fluxes.